



HAL
open science

Towards solar iron metallurgy: Complete hydrogen reduction of iron ore pellets under a concentrated light flux

B. Sanglard, B. Huneau, J. Carrey, S. Lachaize

► **To cite this version:**

B. Sanglard, B. Huneau, J. Carrey, S. Lachaize. Towards solar iron metallurgy: Complete hydrogen reduction of iron ore pellets under a concentrated light flux. *Solar Energy*, 2024, 284, pp.113072. 10.1016/j.solener.2024.113072 . hal-04796801

HAL Id: hal-04796801

<https://hal.science/hal-04796801v1>

Submitted on 1 Jan 2025

HAL is a multi-disciplinary open access archive for the deposit and dissemination of scientific research documents, whether they are published or not. The documents may come from teaching and research institutions in France or abroad, or from public or private research centers.

L'archive ouverte pluridisciplinaire **HAL**, est destinée au dépôt et à la diffusion de documents scientifiques de niveau recherche, publiés ou non, émanant des établissements d'enseignement et de recherche français ou étrangers, des laboratoires publics ou privés.

Towards solar iron metallurgy: complete hydrogen reduction of iron ore pellets under a concentrated light flux

B. Sanglard¹, B. Huneau², J. Carrey¹ and S. Lachaize¹

¹ Laboratoire de Physique et Chimie des Nano-Objets (LPCNO), Université de Toulouse, INSA, CNRS, UMR 5215, UPS, 135 Avenue Rangueil, F-31077 Toulouse, France

² Institut de recherche en Génie Civil et Mécanique (GeM), Nantes Université, École Centrale Nantes, CNRS, UMR 6183, F-44000 Nantes, France

Abstract: Current ironmaking process leads to large CO₂ emissions due to the use of fossil fuels as both heating agent and reducer. An alternative ironmaking process based on the reduction of iron ore by hydrogen under a concentrated light flux, simulating a direct solar heating reactor, is studied here. Experiments were performed in batch mode on the iron ore pellets used in industry, which consist in spherical agglomerates of iron oxide with a diameter of ca. 2 cm. Quantitative analysis of the reduction yield and kinetics were deduced from the Rietveld refinements of X-ray diffraction patterns as well as optical and scanning electron microscopy. It is shown that hydrogen pressure has a significant influence on the time evolution of the reaction, probably by its influence on re-oxydation. Observations and analysis of cut pellets show that reduction starts from the illuminated surface towards the shadowed side, due to a large temperature gradient inside the sample. This conducted us to perform experiments in which pellets were rotated, which significantly reduce reduction time. On single pellets, a reduction yield of 96% was reached in 12 min by turning them three times during exposure. Samples under the form of gravels and flat disks were also tested. The former did not lead to significant improvement, but a 96% reduction yield was measured on 2-mm-thick disks after only 2 minutes of exposure. An analysis of the energy efficiency of the process is provided. These results show that hydrogen-based solar metallurgy could meet industrial requirements in terms of reduction yields and might be envisaged as a low-carbon ironmaking process.

Keywords: Hydrogen, Concentrated solar power, Metallurgy, Iron, Mitigation, CO₂ emissions

31 I. Introduction:

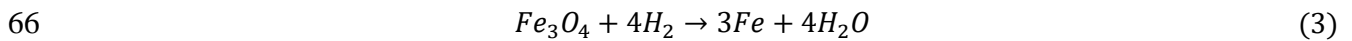
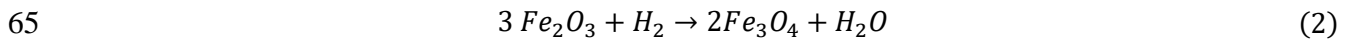
32 Iron and steelmaking industry is responsible for large greenhouse gas emissions, representing
33 close to 6.7% of global anthropogenic CO₂ emissions [1]. Additionally, the ironmaking process
34 has a crucial importance in our society since steel is one of the most used materials worldwide.
35 To respect the +1.5 °C limit of Paris agreement, the emissions from the steelmaking industry
36 should drop from 1.85 t CO₂/t steel to 0.6-0.3 t CO₂/t steel by 2050 in a perspective of a 38%
37 production growth [2]. The most used route to produce steel is the integrated route, which
38 consists in transforming iron ore (mainly composed of hematite and small amounts of magnetite
39 and other mineral oxides) into liquid pig iron (iron-carbon alloy containing up to 5% of carbon)
40 using coal. Some carbon is then removed from pig iron in an oxygen furnace, leading to steel.
41 This route produces alone 71% of the total crude steel used worldwide and emits approximately
42 2.2 tCO₂/t steel [3]. Another well-known and largely used way to produce iron is direct
43 reduction, which consists in a solid-state reduction of iron ore by different reducing gas (CO
44 and/or H₂) at a temperature around 950 °C. The reducing gases mainly originate from coal and
45 natural gas, but can also be produced by biomass pyrolysis [4]. When the reducing agent is
46 carbon monoxide, the reaction contributes to greenhouse gas emissions as shown in Equation
47 (1) [4]:



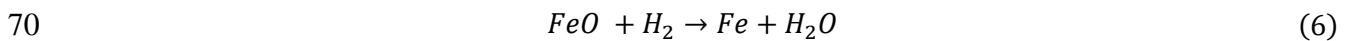
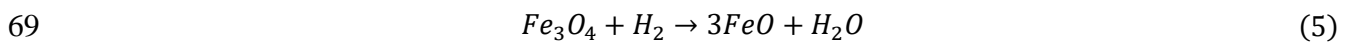
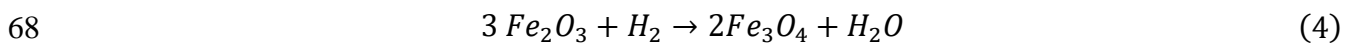
48 The direct reduced iron (DRI) is then melted with carbon in an electric arc furnace to form steel.
49 Globally, direct reduction route leads to lower emissions than the integrated one: 1.95 tCO₂ / t
50 steel and 1.4 tCO₂/ t steel for the coal-based and the gas-based route, respectively [3].

51 Industries and laboratories have investigated several routes to reduce the greenhouse gas
52 emissions of the ironmaking processes. For the integrated route, reduction of the amount of
53 coke used, optimization of the reducer/ore ratio, recycling of the exhaust gas, improvement of
54 the upstream process (coking, smelting) are pathways to diminish the ecological weight of the
55 process [5]. Additionally, Suopajarvi *et al.* have shown that coal consumption and consequently
56 CO₂ emissions could be significantly reduced when partly substituting coal with charcoal,
57 torrefied wood or bio-synthetic natural gas [6]. Unfortunately, they also noted that the
58 production cost of such reducers would be a drawback for this technology. Moreover, the
59 availability of the biomass resource would also be a serious issue.

60 For the direct reduction route, the most studied alternative is based on the use of hydrogen as
61 reducing agent, which forms water as by-product. The reaction goes through different
62 intermediates according to temperature as shown by the Chaudron phase diagram (see
63 Supplementary Information (S.I.) Figure A-1) [4]. For temperatures below 570 °C, magnetite
64 (Fe₃O₄) is formed before reduced iron [7]:



67 For temperatures higher than 570 °C, both magnetite and wustite (FeO) are formed [7]:



71 The reduction of wustite [Equation (6)] is the limiting step of the overall kinetics of the reaction.

72 The use of hydrogen as a low-carbon reducer has already been studied, as reviewed by Heidari
73 *et al.* [8]. Wagner *et al.* showed that the reduction rate rises with temperature [9]. Choi and
74 Sohn studied the high temperature (900-1500 °C) reduction of iron ore small particles (< 100
75 μm) and showed that at 1200 °C the particles were reduced over 90% in 1.6 s with around
76 1000% of H₂ excess. At 1300 °C, around 90% of the reduction was achieved in 2.4 s with 240%
77 of H₂ excess [10]. Hydrogen is also used as reducing agent by companies working with the DRI
78 process (*e.g.* Midrex [11]) and is planned to be more and more used (Hybrit project [12]).
79 Ammonia has also been studied as a carbon-free reducer [16, 17, 18]. For instance, Hosokai *et*
80 *al.* showed that 0.27 g of pure hematite could be reduced completely at 600°C and 700°C after
81 respectively 2h and 1h.

82 However, the hydrogen route is intensive in electricity when green hydrogen – i.e. produced by
83 electrolysis using low-carbon electricity – is used. Indeed, the energy consumption to produce
84 iron from green hydrogen represents 3.5 MWh/t steel, with approximately 70% due to the
85 production of green hydrogen itself [14]. As comparison, the integrated route uses 356 kWh/t
86 steel and the DRI route 1.2-1.3 MWh/t steel [3]. Among the later, the melting of the DRI in
87 the EAF furnace is the main item of consumption : it has been estimated to 918 kWh/t of steel
88 by Fan *et al.* [3] and to 753 kWh/t by Vogl *et al.* [14]. Provided that 1.9 Gt of steel were
89 produced in 2023 [15], maintaining the current level of iron production with green hydrogen

90 would require 6 622 TWh of low-carbon electricity. This value corresponds to 22% of the
91 electricity produced worldwide the same year (29 471 TWh in 2023) [16]. Providing such an
92 amount of low-carbon electricity in a few decades is a huge challenge, to say the least.

93 As already mentioned above, another way to reduce emissions in the integrated or DRI route
94 would be to change the classically used coke to biochar or biogas. However, biomass resources
95 – as low-carbon electricity – are also limited and should be shared with other industrial sectors.
96 So decarbonating iron production at our current level of production in a few decades seems
97 difficult; with a view to a sustainable future, it might even not be desirable to keep such a high
98 level of production in reasons of the global upstream and downstream social and environmental
99 impacts of iron (mining, artificialisation, infrastructures, ...). Thus, an approach based on a
100 more efficient steel use, on reuse and on low contamination recycling would lead to a decreased
101 level of production, complementary of any low-carbon process. Sufficiency and lifestyle
102 changes are also additional ways to induce a significant production decrease [17].

103 To efficiently reduce the CO₂ emissions of the DRI process, the contributions originating of
104 both heat production and chemical reaction should be tackled. In this work, it will be studied
105 the use of concentrated light flux to provide heat and hydrogen as reducer.

106 In this perspective, the use of solar concentrated power as a heat source has been studied before.
107 For instance, in 1991, Steinfeld and Fletcher studied direct carbothermic reduction (reduction
108 of hematite with solid carbon) under concentrated solar flux and were able to reach 78% of
109 reduction yield at 2000 K [18]. In 1993, Steinfeld and Kuhn studied the reduction of magnetite
110 (Fe₃O₄) under concentrated solar flux and methane atmosphere [19]. They were able to reach
111 68% of reduced iron from a dry mixture of magnetite and silica after heating it during 15
112 minutes at 1273 K in a solar oven. Fernández-González *et al.* studied the smelting reduction of
113 hematite (Fe₂O₃) with carbon under solar flux and the one of sintered ore with coke breeze [20].
114 They were able to reach a maximum of 5.6% of reduced iron in the hematite sample at 1353 °C
115 and 29.7% in the sintered oxide one, reaching a temperature high enough to melt the upper layer
116 of the sample.

117 So far, only two studies of the combined use of hydrogen and solar energy for direct reduction
118 has been recently published : Li *et al.* [21] and Abanades *et al.* [22]. First, Li *et al.* studied the
119 reduction under hydrogen of hematite fine particles in an indirect solar heating reactor equipped
120 with a vibrant fluidized bed and were able to reach 98% of reduction in 50 min. Secondly,
121 Abanades *et al.* studied the reduction of iron ore power (from 0.25 to 2 mm in diameter) in

122 backed bed under solar irradiation. They showed a complete reduction after 15 min at 1000 °C
123 and showed that the quantity of powder in the backed bed had an influence on the reduction
124 rate.

125 The experiments described hereafter differs from both studies. First, they were conducted on
126 the exact same pellets as the one used in industrial processes whereas iron ore powder or hematite
127 powder was used in the previous studies. Secondly, here, the reduction was realized by exposing
128 directly the sample to concentrated light flux (direct reactor) where Li *et al.* and Abanades *et*
129 *al.* used an indirect reactor. Moreover, in this work, several experimental parameters of the
130 reduction were varied in order to understand the reaction mechanisms and to reach high
131 reduction yield in a short time.

132 This article is organised as follows. First, test bench, samples and methods are described.
133 Second, the influence of various parameters (pressure, time, power) is shown. Third, results to
134 optimize the reduction time and yield are presented, as well as an energy analysis. Finally, the
135 results are discussed before providing a general conclusion.

136 II. Materials and methods:

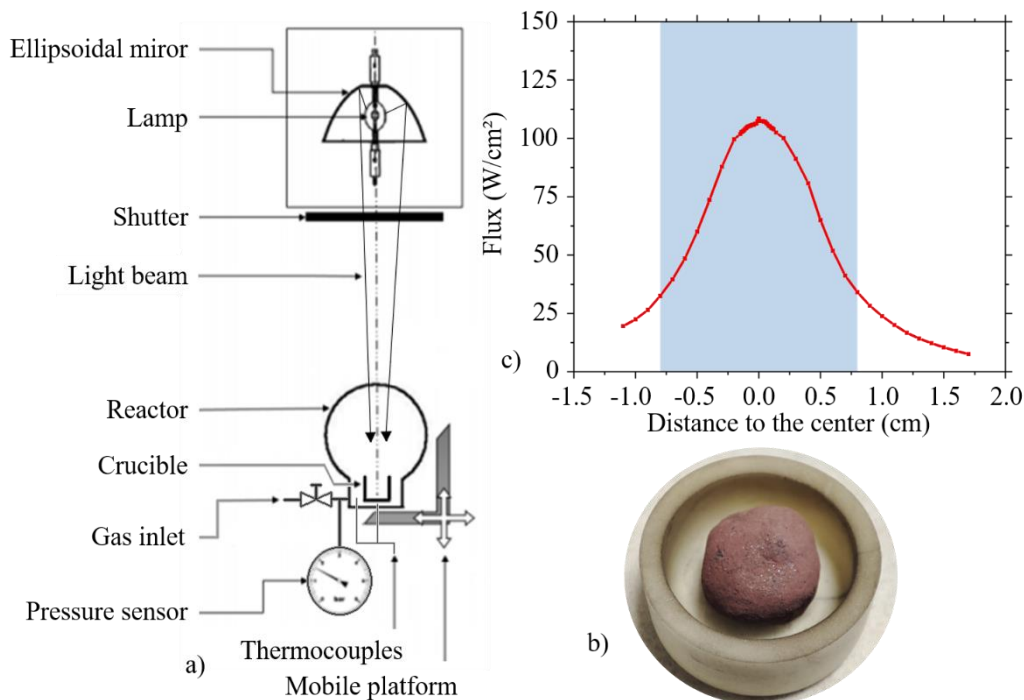


Figure 1: (a) Schematic of the solar simulator bench used for the experiments. (b) Detail picture of the crucible holding a typical iron ore pellet (crucible A). (c) Light flux measurement over the crucible radius.

137 Experiments were realised using the experimental set-up shown in Figure 1-a. The bench is
138 composed of a Xe lamp (electric power of 1600 W_e, 9 mm long arc) placed at the focal point of
139 an ellipsoidal mirror (XE1600, Sciencetech). The total light power at the output of the reflector
140 was calculated by performing a series of flux measurements (flux meter TG1000-0, Vatell) over
141 the complete radius of the light spot (see Figure 1-c). The total power is then obtained after an
142 integration of the curve. An alumina crucible (diameter: 16 mm, Sceram ceramics) is placed
143 inside a 0.6 L borosilicate glass reactor resistant to 10 bars of gas pressure. This reactor is placed
144 on a mobile XY platform (Thorlabs – two XR25C mounted at 90°), the displacement over the
145 Z axis being realised with a homemade rack and pinion. The crucible was placed a few
146 centimetres below the focal point to be more homogeneously illuminated. At this position, a
147 power of about 140 W was measured, corresponding to a mean flux of 70 W/cm² (see Figure
148 1-c). The temperature is measured with two K-type thermocouples: one placed right under the
149 crucible and the other one in the atmosphere but not directly under the light flux. The pressure
150 inside the reactor is measured with a sensor (type 520, Huba control). Both temperature and
151 pressure are acquired in real-time using a homemade Labview program. Before each
152 experiment, the reactor is successively vacuumed and refilled three times with the reducing gas
153 before setting it at the required pressure; each experiment was thus performed under a static
154 atmosphere condition. The hydrogen is produced by water electrolysis using a H₂ generator (F-
155 DGSi, model WM-H2, O₂ < 0.01 ppm and moisture < 1 ppm). After the experiment, samples
156 are left to cool before being placed in the ambient atmosphere and analysed.

157 The samples used for the experiments were industrial grade iron ore pellets used in the DRI
158 process, courtesy of the ironmaking company ArcelorMittal (Metz, France). They are mainly
159 composed of iron oxide (> 97%) with a small amount of standard impurities (Si, Al, Ca, MgO).
160 The composition provided by the furnisher can be found in S.I. Table B-1.

161 First, reduction experiments under different conditions were realised by placing the sample in
162 a 2.0 cm² area crucible (crucible A, see Figure 1-b) under several pressures and exposure times.
163 The pressure studied were 1, 2 and 4 bars to determine which minimal pressure was acceptable
164 to ensure the sample reduction and to prevent its re-oxidation by the water vapor produced
165 during reduction [19], [23]. The maximum of 4 bars allows to be far from the safety limit of
166 our glass reactor even at the end of the experiments since pressure increases all along the

167 reduction process. Additionally, the longest exposure time of 28 minutes was chosen after
 168 preliminary experiments showing a significant reduction yield of iron ore powder after this
 169 duration. For these series of experiments, only the quantitative advancement of the reduction
 170 was studied and not the reduction yield itself. To this end, the samples were dried before the
 171 experiments at least 1 week into a proofer at 110 °C and weighted before and after reduction.
 172 This allowed to access the oxygen loss value, which is a good indicator of the quantitative
 173 advancement of the reduction.

174 Other experiments were realized to observe specifically the way the reduction proceeds inside
 175 the samples. Firstly, the exposure time was varied from 0.5 min to 16 min under 60 W/cm².
 176 Secondly, 4 min reductions under different mean light density flux values were performed
 177 (46 W/cm², 54 W/cm², 60 W/cm², 65 W/cm² and 75 W/cm²). For each varied parameter,
 178 measurements were realised on two series of pellets. In each series, their masses differed by
 179 less than 5% (see Table 1). The pellets were cut in half vertically and observed using optical
 180 microscopy. The surface of the iron phase compared to the oxide one was measured using
 181 ImageJ software by contouring each surface. EDX mapping was also realised using a SAMx
 182 detector on a JEOL 6060-LA SEM.

183 *Table 1 : Conditions of the performed reduction experiments.*

Varied parameter	Variation	Samples	Masses (g)	Mean diameter (cm)	H₂ pressure (bar)	Note
Exposure time	0.5 to 16 min	Serie 1	2.11 to 2.19	1.05	2	60 W/cm ²
		Serie 2	2.29 to 2.38	1.14	2	
Light power density	46 to 75 W/cm ²	Serie 3	2.18 to 2.25	1.13	2	4 min reductions
		Serie 4	2.33 to 2.38	1.13	2	

184
 185 Finally, the reduction yield of the process was assessed and different ways were tested to reach
 186 high enough values with respect to industrial requirement (approx. 93-94% for the DRI process
 187 [24], [25]). To this end, the initial shape of the raw materials was changed into gravel or disks,
 188 by either grinding the pellet or by cutting it using a precision circular saw with diamond blade
 189 (Buehler IsoMet low speed saw; Buehler – n°114254). Experiments on disks were conducted
 190 using a specifically designed crucible (crucible B, see S.I. Figure E-3): it favours gas circulation
 191 by avoiding a direct contact between the bottom surface of the disk and the crucible; it also
 192 avoids shading the disk by the crucible walls.

193 To measure the reduction yield, samples were transformed in powder using mortar and pestle,
194 and then analysed using an X-ray diffractometer (PANalytical Empyrean 45 mA 35 kV, Co).
195 For experiments on pellets, the quantity of analysed powder represented between 1/4 and 1/3
196 of the pellet. For experiments on gravels, all the gravels present in the crucible were transformed
197 into a powder which was analysed. Afterwards, Highscore software was used to identify the
198 phases within the sample; MAUD software was then used to realize Rietveld refinements on
199 the diffractograms to access the mass percentage of each phase. When the refinements were
200 used, the contribution of the residual peaks was less than 1%. Finally, the experimental
201 reduction yield was calculated by dividing the mass of metallic iron after reduction by the mass
202 of iron-containing phases in the sample before reduction, as shown by Equation (7).

$$203 \quad \text{Reduction yield} = \frac{\%_{Fe(0)}}{\%_{Fe_2O_3} + \%_{Fe_3O_4} + \%_{FeO} + \%_{Fe(0)}} \quad (7)$$

204 III. Results and discussion

205

206 III.1. Influence of pressure, exposure time and lamp power on reduction 207 performances

208 Figure 2 presents the results of iron ore reduction under a solar simulated flux as a function of
209 exposure time for different hydrogen pressures. The oxygen mass loss analysis was realised
210 following the previously presented protocol. The interest of this analysis is to allow for a quick
211 observation of the effect of experimental parameters on the reduction rate. At first sight, it can
212 be observed in Figure 2 that the oxygen loss rises steeply during the first 4 min without
213 significant influence of pressure. Afterwards and until 8 min the steepness of the curves lowers
214 slightly but still without major influence of pressure. After 8 min, the curves split: the 4-bar
215 curve continues to rise with a decrease in the steepness; the 2-bar curve plateaus; the 1 bar curve
216 decreases. The splitting of the curves during the reaction is attributed to hydrogen consumption
217 [26]; theoretically, to completely reduce one equivalent of Fe^{3+} , 1.5 equivalents of H_2 are
218 necessary. At the beginning of the reaction, the $H_2:Fe$ ratios are 1.55:1, 2.35:1 and 3.89:1 at 1,
219 2 and 4 bars respectively (the ratios were calculated using the iron oxide masses, the reactor
220 volume and the stoichiometry of the reaction). Thus, at 1 bar pressure, there is only a small
221 excess of hydrogen compared to the theoretical value. So, as the reduction progresses and because
222 the experiments are realised in batch, the competition between the water vapor formed and the

223 remaining hydrogen lowers the activity of the latter, as previously discussed in the literature
224 [27]. The decrease after 8 min of the 1 bar curve is interpreted as a re-oxidation of the sample
225 due to the presence of a large excess of water. This behaviour has previously been reported for
226 magnetite at temperatures between 100 and 500 °C [18, 21].

227

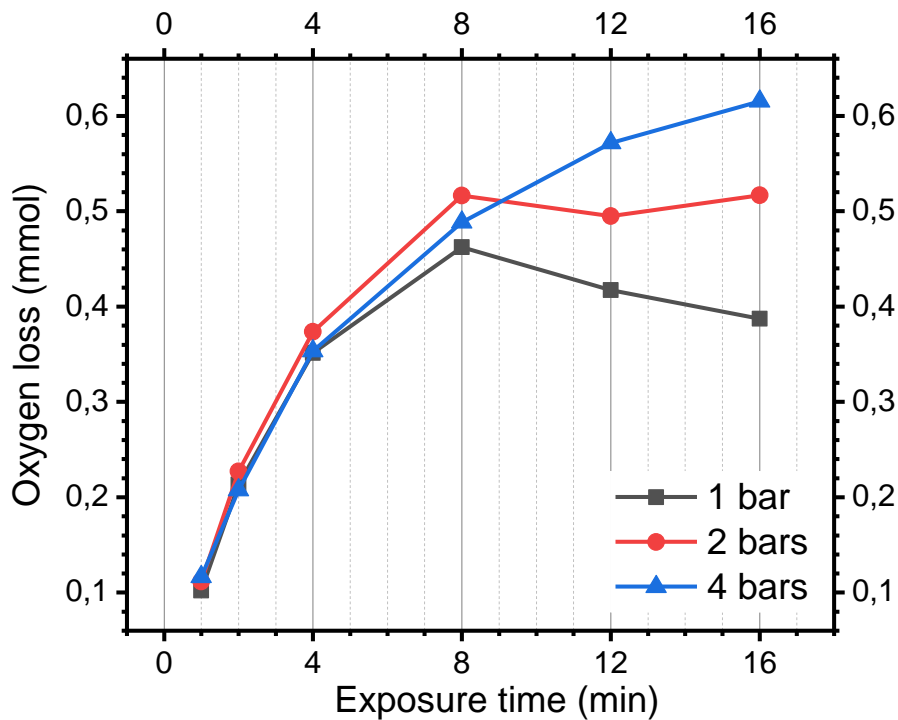


Figure 2: Oxygen loss as a function of the exposure time for various pressures of hydrogen (black: 1 bar; red: 2 bars; blue: 4 bars) after reduction of iron ore pellets under 60 W/cm². Each point of the curves represents a complete experiment.

228 Since the light flux is concentrated onto the top of the sample, the conditions are drastically
229 different from a classic furnace. Therefore, it was decided to cut the reduced pellets in half (as
230 shown in Figure 3-a) to observe the progression of the reduction front. Figure 3-b and c show
231 the inside of two pellets exposed to the light flux during 2 and 7 min, respectively, the red line
232 representing the reduction front. In the pictures, two zones with very different colours are
233 observed. SEM observations coupled with EDX mapping show that the upper part (above the
234 red line) of the sample is iron whereas the lower one (under the red line) is iron oxide.
235 Quantitative analyses show that the transitions between the two materials occurs within ca. 0.5
236 mm (see S.I. Figures C-1). In a standard oven, the reduction of pellets is usually described by
237 the shrinking core model: the reduction starts from the external surface of the pellets and goes
238 towards the core of the pellets, thus creating an iron shell [28]. Here, the behaviour is different:
239 because of light irradiation, the reduction starts from the top of the pellet and grows downwards,

240 hence preserving the iron oxide in the shadowed side of the pellet. The reduction being
241 temperature dependent, this reveals the presence of a temperature gradient within the pellet.

242

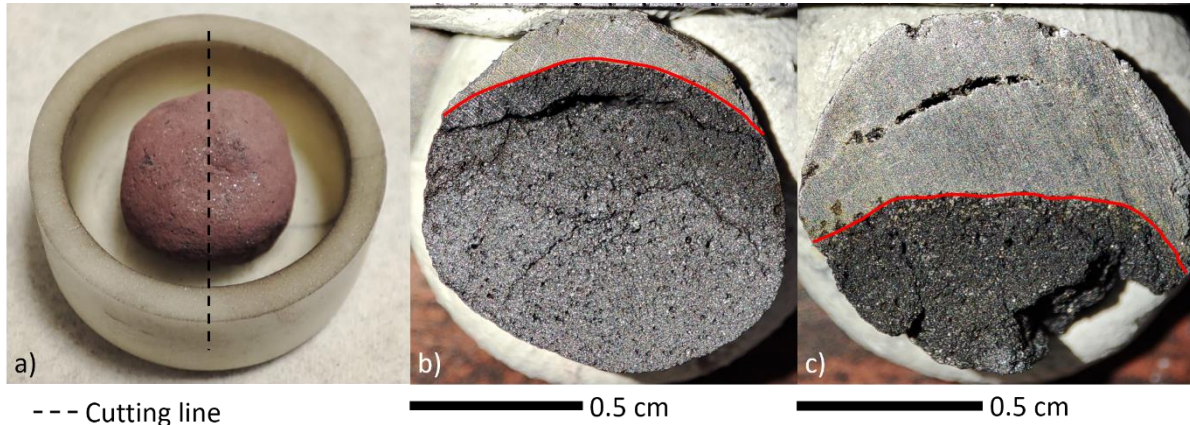


Figure 3: (a) Picture of a pellet in the crucible. The dotted line represents the profile on which the pellets were cut in half. Picture of a pellet after hydrogen reduction during (b) 2 min and (c) 7 min under 2 bars of hydrogen and 60 W/cm². The pellet was cut in two after the experiments to perform this observation. The red line represents the reduction front with the reduced iron above and the iron oxides below. Samples were illuminated from the top.

243 To quantify this progression, the surface of reduced iron for an exposure time varying from 0.5
244 min to 16 min as well as the total surface of the pellets were measured (see Figure 4). The
245 surfaces were determined using the software ImageJ on images such as the ones shown in
246 Figure 3-b and Figure 3-c. The corresponding pictures are available in S.I. Figures C-2 and C-
247 3. Results show that the reaction rate follows an exponential decay tendency, plateauing or
248 strongly slowing down after 10 minutes, before the reduction is complete. These pictures can
249 also be used to estimate the reduced thickness per unit of time: it evolves from 2 mm/min at the
250 very beginning to 0.3 mm/min before the plateau (between 7 and 10 min of reaction). Such a
251 behaviour has previously been observed in the hydrogen reduction of pellets in an oven, and
252 was interpreted as due to the slower diffusion rate of hydrogen in the reduced iron as opposed
253 to the one in the porous oxide [29]. However, here, since the bottom of the pellet is clearly not
254 reduced, hydrogen keeps its capability to feed the reaction toward the reduction front at the same
255 rate. This result is therefore interpreted as resulting from a temperature gradient appearing
256 inside the pellet and will be discussed more thoroughly in section III.3.

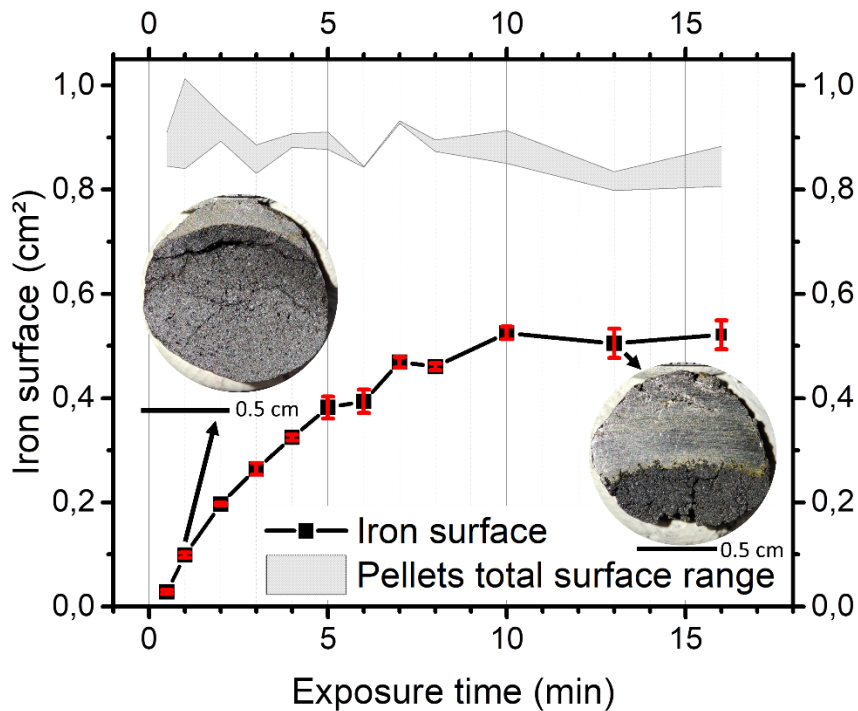


Figure 4: Iron surface evolution as a function of exposure time after the reduction of pellets under 2 bars of hydrogen and 60 W/cm² (square dots). The black line corresponds to the iron surface averaged over the two series, and the error bar to the standard deviation. The total surface of each of the two pellets used to measure one point is indicated as two grey-filled curves. Pictures of cut samples exposed for 2 min and 13 min are shown as insets.

257 Figure 5 shows the evolution of the iron surface as a function of the light flux density for 4 min
 258 of reduction under 2 bars as well as the total surface of the pellets. The later were cut as shown
 259 in Figure 3-a and corresponding pictures are shown in S.I. Figures D-1 and D-2. The surfaces
 260 were here again determined using the software ImageJ. As expected, the reduced surface
 261 increases with lamp power, evidencing the influence of temperature on reduction rate.

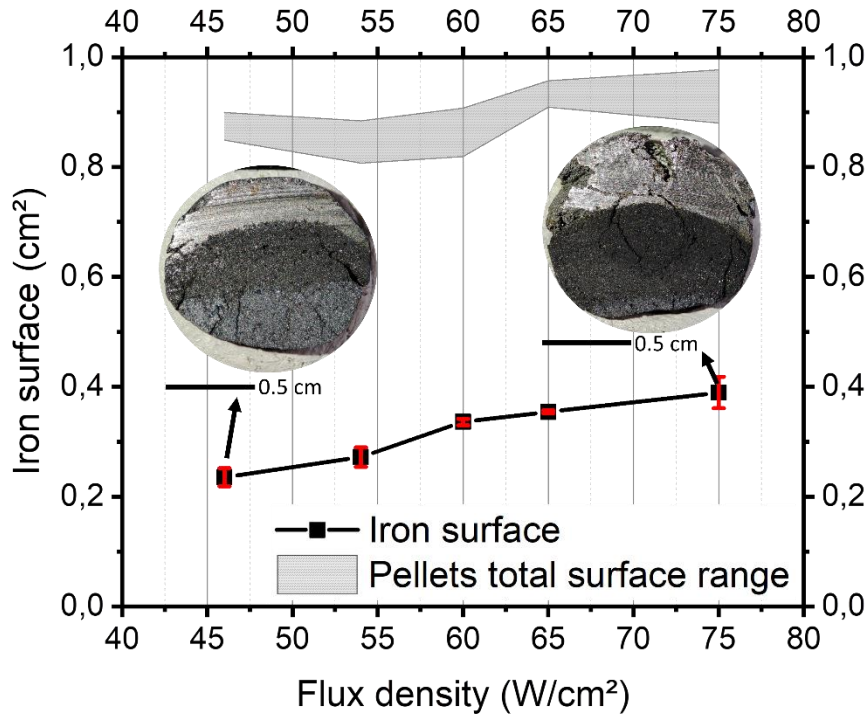


Figure 5: Iron surface after 4 min reduction under simulated solar flux and 2 bars of hydrogen for several light flux density: 46 W/cm², 54 W/cm², 60 W/cm², 65 W/cm² and 75 W/cm². The total surface of the pellets is indicated as two grey-filled curves. The black line corresponds to the iron surface averaged over the two series and the error bar to the standard deviation. Pictures of cut pellets for 46 W/cm² and 75 W/cm² are shown as insets.

262 III.2. Optimization of reduction yield and kinetics

263 The reduction rates observed in these experiments were of the same order of magnitude as the
 264 one found in the literature on hydrogen reduction [30], [31]. Nonetheless, in order to try to
 265 reduce exposure times, experiments consisting in turning over the pellets one or three times by
 266 180° or 90°, respectively, were conducted. Similar experiments were also conducted on gravel.
 267 In the latter case, they were only shaken until a majority of them were turned. For experiments
 268 on both pellets and gravel, crucible A was used and the samples were allowed to cool down
 269 before being manually turned over radially or shaken.

270 Finally, optimization was attempted on three types of samples in order to study the impact of
 271 sample shape on the reduction yield and kinetics: i) pellets, ii) a single-layer of gravel of ca. 2.0
 272 mm and iii) 2.0 (± 0.11) mm thick disks with different mean radius (7.7 mm, 5.9 mm and 4.5
 273 mm). Since their thicknesses are similar, the disks are listed as function of their radius. Pictures
 274 of the gravel and the disks are available in S.I. Figures E-1 and Table E-1 respectively. Table 2
 275 summarizes the structural properties of the various samples (pellets, gravel and disks), the
 276 experimental conditions, as well as the main results.

277 *Table 2: Structural properties, experimental conditions and main results in the series of*
 278 *experiments aiming at maximizing the reduction yield (XRD quantification) under hydrogen*
 279 *atmosphere. The lamp flux density was 60 W/cm². A reactor with a constant volume of 0.6 L*
 280 *was used. For the temperature, the one of the disks are not informative because of the specific*
 281 *configuration of the experiments (cf S.I. Figure E-3).*

<i>Sample</i>	<i>Sample type</i>	<i>Initial mass (g)</i>	<i>Pressure (bar)</i>	<i>Total exposure time (min)</i>	<i>Reduction yield (%)</i>	<i>Wustite percentage (%)</i>	<i>Temperature under the crucible (°C)</i>	<i>Note</i>
<i>S1</i>	<i>Gravel</i>	<i>0.37</i>	<i>2</i>	<i>28</i>	<i>88.4</i>	<i>11.6</i>	<i>412</i>	
<i>S2</i>	<i>Gravel</i>	<i>0.31</i>	<i>2</i>	<i>28</i>	<i>94.7</i>	<i>5.3</i>	<i>389</i>	<i>Turned over once by approx. 180°</i>
<i>S3</i>	<i>Pellet</i>	<i>1.70</i>	<i>3.5</i>	<i>28</i>	<i>83.8</i>	<i>14.5</i>	<i>371</i>	
<i>S4</i>	<i>Pellet</i>	<i>1.71</i>	<i>3.5</i>	<i>28</i>	<i>97.3</i>	<i>2.7</i>	<i>380</i>	<i>Turned over once by approx. 180°</i>
<i>S5</i>	<i>Pellet</i>	<i>1.90</i>	<i>2</i>	<i>16</i>	<i>95.1</i>	<i>4.9</i>	<i>371</i>	<i>Turned over once by approx. 180°</i>
<i>S6</i>	<i>Pellet</i>	<i>1.92</i>	<i>2.4</i>	<i>17</i>	<i>99.0</i>	<i>1.0</i>	<i>351</i>	<i>Turned over thrice by approx. 90°</i>
<i>S7</i>	<i>Pellet</i>	<i>1.94</i>	<i>2.4</i>	<i>12</i>	<i>95.1</i>	<i>4.9</i>	<i>323</i>	<i>Turned over thrice by approx. 90°</i>
<i>S8</i>	<i>Disk</i>	<i>1.24</i>	<i>2</i>	<i>2</i>	<i>73.5</i>	<i>23.5</i>	<i>-</i>	<i>Radius: 7.70 mm</i>
<i>S9</i>	<i>Disk</i>	<i>0.71</i>	<i>2</i>	<i>2</i>	<i>96.0</i>	<i>3.9</i>	<i>-</i>	<i>Radius: 5.90 mm</i>
<i>S10</i>	<i>Disk</i>	<i>0.45</i>	<i>2</i>	<i>2</i>	<i>92.7</i>	<i>6.3</i>	<i>-</i>	<i>Radius: 4.50 mm</i>

282

283 III.2.1. Pellet reduction

284 Sample S3 is considered as the reference sample: a non-turned pellet exposed to the light flux
 285 during 28 min under 3.5 bars of hydrogen. The temperature profile measured by the
 286 thermocouple under the crucible shows a maximum of 371 °C at the end of the experiment (see
 287 S.I. Figure E-2). The XRD diffractogram of the reference sample after reduction is provided in
 288 S.I. Figure D-3. The reduction yield deduced from the refinement of the curve is 84%, which is

289 too low for an industrial application. In order to improve the efficiency of the process, the pellet
290 was turned upside down after 14 min of reduction (sample S4), increasing the yield up to 97%.

291 Then, the possibility i) to reduce the exposure time and ii) to lower the hydrogen pressure was
292 tested to see if it could still lead to an acceptable yield. Provided that no re-oxidation was
293 observed at 2 bars for a pellet of around 2.83 g (see Figure 2), the pressure value was kept at
294 2 bars or 2.4 bars depending of the pellet mass. As shown in Figure 3, a 7 min reduction is
295 expected to be sufficient to reduce half the pellet. Sample S5 was therefore reduced during two
296 sets of 8 min and was rolled over in between, leading to a reduction yield of 95.1%. Here, a
297 difference between the highest temperature before (357 °C) and after (371 °C) the rolling over
298 is observed. This small difference is probably due to the higher thermal conductivity of metallic
299 iron compared to magnetite.

300 Finally, it was tested to rotate the pellet 3 times by approx. 90° and to expose it 4 min only
301 between rotations. Samples S6 and S7 show reduction yields of 99.0 % and 95.8% for a total
302 exposure time of 17 min and 12 min, respectively. The XRD diffractogram of sample S6 is
303 available in Figure S.I. D-4. This evidences that rotating pellets under the concentrated light
304 flux remarkably increases reduction yield and/or decreases reduction time. With regards to
305 temperatures, as for sample S5, a difference in the reached temperature was observed between
306 each phase of the experiment. For S6 the maxima were 313 °C, 329 °C, 351 °C and 348 °C; for
307 S7 they were 302 °C, 315 °C, 323 °C and 322 °C. Here again, the general trend observed is
308 attributed to the higher conductivity of metallic iron. For both samples, the temperature reached
309 during the last part of the reduction is close to the temperature reached during the previous one.
310 This could mean that the reduction is mostly complete after the third phase of the experiment.

311 One should note that the temperatures measured under the crucible are relatively low compared
312 to the one allowing a fast and complete reduction [32]. However, it is important to keep in mind
313 that the top of the pellet is directly illuminated so it reaches much higher temperatures. As
314 example, during preliminary experiments, a pyrometer was used to measure the surface
315 temperature of powder samples; it was saturated, which indicated temperatures higher than
316 900 °C. This issue will be fully discussed in section III.3.

317 XRD analysis of all the samples indicates that, when the reduction is well advanced, the sample
318 is composed of iron and wustite only. This is the case for samples S2, S4, S5, S6, S7, S9 and
319 S10. Nevertheless, for less reduced sample (S1, S3 and S8) the sum of wustite and iron does
320 not reach 100%, as shown in Table 2. The difference is the amount of magnetite in the sample.

321 For these samples, the temperature was not high enough to fully reduce magnetite into wustite
322 at the end of the experiment.

323 III.2.2. Gravel reduction

324 In order to lower the reduction time further, gravels were studied. A single layer of gravel was
325 placed at the bottom of the crucible in order to ensure a complete exposition of the samples.
326 The temperature profile during the experiment on non-turned gravels is available in S.I. Figure
327 E-2. It can be observed that the highest temperature measured under the crucible was 412 °C.
328 XRD analysis evidences that the reduction yield was 88.4% after 28 min, the remaining oxide
329 being wustite only (see Table 2). The second experiment was conducted with the same total
330 exposure time but the gravels were shaken to turn them over after 14 min. A reduction yield of
331 95% was obtained, which fulfils industrial requirements but remains slightly lower than the one
332 obtained on pellets. The relationship between the reduction yield and the measured temperature
333 under the crucible will be discussed in section III.3.

334 III.2.3. Disk reduction

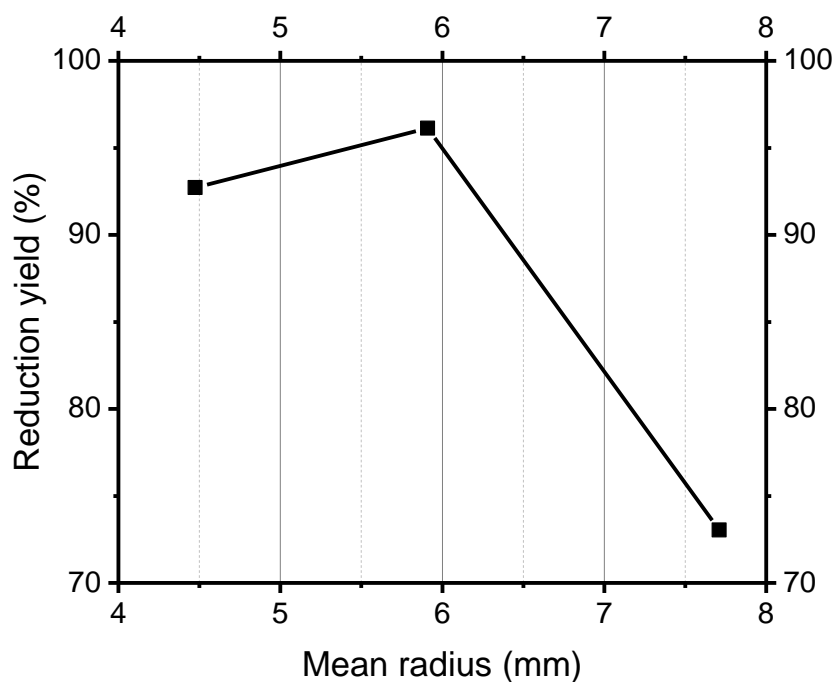


Figure 6: Reduction yield of disks cut into industrial iron ore pellets as a function of their mean radius. The lamp flux density was 60 W/cm², hydrogen pressure 2 bars and reduction time 2 min.

335 Experiments conducted on pellets have shown that the reduction front has moved of ca. 2 mm
336 after 2 min of exposure (see Figure 4). In order to optimize the process, disks with a thickness

337 of 2 mm were cut and studied. The XRD diffractograms of samples S8, S9 and S10 after
338 reduction are available in S.I. Figures E-4, E-5 and E-6, respectively. They show the presence
339 of wustite and magnetite for S8 and S10, with more intense peaks in the case of S8. Figure 6
340 shows the reduction yield of the disks after 2 min of exposure under 2 bars of hydrogen.

341 Large reduction yields of 92% and 96% were obtained for the disks with a radius of 4.75 mm
342 and 5.90 mm, respectively, matching industrial requirements. However, a significant decrease
343 down to 73% occurs for the sample with a radius of 7.70 mm. This decrease was assumed to be
344 related to the non-homogeneity of the light flux in the disk plane. The area where the light flux
345 is more intense is approximately 6 mm in diameter (see Figure 1-c) and can be identified as the
346 whitest spot on the disk in S.I. Table E-1.

347 Overall, results from section III.2 show that the shape of the iron oxide materials significantly
348 affects reduction time. It is possible to reach low reduction times and large reduction yields
349 when the thickness is reduced. Here, the exposure time was divided by a factor of 14 when
350 going from a 3D sample (single pellet exposed during 28 min) to a 2D one (disk exposed during
351 2 min). With respect to production rate, it increased by a factor 6 (0.06 g/min to 0.36 g/min)
352 when going from pellet to disk. This shows that the sample size and shape is a really important
353 parameter in the performance of the process.

354 III.2.4. Energetical efficiency

355 For the sake of comparison with future developments and other processes, the energy efficiency
356 of the experiments was estimated. Efficiencies were calculated for the most representative
357 cases: the pellet not turned over (S3), one of the pellets turned over (S7) and one of the disks
358 (S9). The efficiency is defined as the theoretical energy required to heat and reduce the sample
359 (E_{th}) divided by the measured energy of the incoming light on the area of the crucible (E_l), as
360 explained in section II. Details on the calculations are provided in S.I. section G. Results are
361 displayed in Table 3 for three temperatures ranging from 500 °C to 1500 °C. The lower bound
362 of this range corresponds to the lowest temperature allowing a complete reduction [33]. The
363 upper bound is the fusion temperature of iron, which was never observed in any of our
364 experiments. As expected for experiments performed on single objects in a non-thermally
365 optimized reactor, the absolute efficiency values are quite low due to thermal losses by radiation
366 and convection. However, the efficiency values increase by a factor 6 (respectively 2.47)
367 between S3 and S9 (respectively S7), evidencing quantitatively the interest in turning the pellets
368 or using flat samples.

369 *Table 3 : Energy to heat and reduce the sample (E_{th}), energy output of the simulator for each*
 370 *sample (E_l) and energy efficiency as the ratio between the two values.*

Sample	E_{th} (J)			E_l (J)	Efficiency (%)		
	500 °C	1000 °C	1500 °C		500 °C	1000 °C	1500 °C
S3	971	1505	2039	201600	0.48	0.75	1.01
S7	1142	1751	2360	86400	1.32	2.03	2.73
S9	424	647	870	14400	2.95	4.49	6.04

371

372 III.3. Discussion

373 In the present section, three worthwhile points will be discussed: i) the temperature of the
 374 samples and its link with the reduction mechanism, ii) the scaling-up and potential
 375 industrialisation of such a process, and iii) the potential environmental interest of such process.

376 In the process studied here, the pictures of the cut pellets (see Figure 3-a and 3-b and S.I. Figures
 377 C-2, C-3, D-1 and D-2) show that the top of the pellet react first. One could think to two
 378 hypotheses to explain it, related to two different limiting factors: i) the temperature is larger at
 379 the top ii) the hydrogen does not reach easily the bottom of the pellet because it is sunk into the
 380 crucible. The second hypothesis has been excluded by performing an experiment where a pellet
 381 was hold onto the top of a small tripod, without any potential limit to hydrogen access. No
 382 change in the asymmetry of the reduction was observed, indicating that the limiting factor of
 383 the reduction process is temperature and not hydrogen diffusion around the pellet. The
 384 mechanism of diffusion of the hydrogen into the pellets is well known. It consists of a mass
 385 transfer of the gaseous hydrogen from the atmosphere to the surface of the pellet, followed by
 386 a diffusion of the gas through the macro- and micropores of the pellet to reach the active sites
 387 and reduce the oxide. The water vapor exits in the opposite way [32], [34]. Additionally, when
 388 iron is formed around the sample, is it possible for hydrogen to diffuse through it [32], [34].

389 The clear frontier between the iron oxide phase and the iron(0) observable on all the pictures of
 390 cut pellets suggests the presence of an isotherm. The heat being provided by a direct
 391 illumination of the samples, having access to the temperature of this isotherm is not an easy
 392 task as the temperature is expected to be strongly inhomogeneous. In experiments (not shown)
 393 where the top surface temperature of the sample has been measured using a pyrometer, values
 394 above the upper limit of our apparatus (900 °C) were obtained. Since the iron formed at the top
 395 of the pellet has not melt during any of the experiments, the temperature necessarily stays below

396 1500 °C (iron fusion temperature). On the other hand, the temperature measured just below the
397 crucible (see Figure 1-a) after 28 min was 371 °C for the pellet (see S.I. Figure E-2). Thus, the
398 temperature of the sample during the reaction lies between 1500 °C and this last value (371 °C).
399 A rough estimate of the isotherm value is provided by combining the reduction front speed
400 deduced from Figure 4 (2 mm/min at the beginning and 0.3 mm/min before reaction plateaus)
401 and the experiments by Turkdogan et Vinters on the link between reaction temperature and size
402 of pellets [35]. Using their data, it is estimated that the isotherm value varies from above
403 1000 °C at the beginning of the reaction to roughly 800 °C when the front speed equals 0.3
404 mm/min.

405 For the reduction of gravel, it might, at first sight, seems counter-intuitive that the temperature
406 measured under the crucible was higher for the gravel than for the pellet (412 °C vs 371 °C; cf
407 S.I. Figure E-2) whereas the reduction yield was smaller. This observation could be explained
408 by several phenomena: i) a smaller temperature gradient due to the smaller size of the gravel,
409 ii) an increase of thermal losses due to their larger surface-to-volume ratio, iii) an incomplete
410 coverage of the crucible by the gravel so that parts of its bottom are directly exposed to the light
411 flux, iv) a slow-down of the reduction rate for small samples as observed previously by
412 Turkdogan et Vinters [35] and v) the heat stored by the gravel because of the smaller mass of
413 the sample. Presently available experimental data are not sufficient to decide between these
414 various hypotheses.

415 In term of scale-up, high concentration ratio technologies like dish or central receivers produce
416 large enough temperature (> 800 °C) to allow hydrogen-based reduction. Given the results
417 provided in the present article, it seems that two different types of reactors could be considered
418 when working with a direct concentrated solar flux. Firstly, moving reactors like rotary kiln or
419 rotating cylindrical reactor have already been studied for high temperature concentrated solar
420 based thermochemical process [36], [37], [38]. This kind of reactor could allow for an
421 advantageous random but continuous rotation of the pellets since it has been shown here that
422 the slowing down of the reaction can be overcome when rotating the pellets. Secondly, in the
423 view of the results with the disk samples, a new reactor in which a few millimetre-thick plates
424 or chips of iron oxide would slide through the light flux on a conveyer belt type reactor could
425 potentially be interesting. These paths will be explored in future experiments.

426 Solar facilities only count on renewable energy during their use phase, which is a clear
427 advantage compared to the fossil-fuel based equivalent processes. However, such solar facilities
428 are generally much more material-intensive and therefore energy-intensive during their

429 building phase than standard processes due to the necessity to produce and hold in place large
430 areas of reflectors. The potential savings of CO₂ emissions and reduction of other environmental
431 impacts of solar metallurgy should be studied using life cycle assessment. This will be the
432 subject of future studies. As a preliminary study, our group has recently shown that cooking
433 with parabolic solar cookers compared to standard devices strongly reduce impacts [39]. It is
434 possible to provide a very rough range for the CO₂ emissions of a potential hydrogen-based
435 solar process. As recalled in the introduction, a non-solar hydrogen-based electrically-produced
436 steel consumes 3.5 MWh/t, among which 70% comes from the hydrogen production, the
437 remaining being the energy to heat the ore and melt the DRI [14]. With a low-carbon electricity
438 mix such as the French one (86 gCO_{2eq}/kWh [40]), the non-solar process would emit
439 301 kgCO_{2eq}/t of steel. With a carbon intensive electricity mix such as the Australian one (943
440 gCO_{2eq}/kWh [41]), the impact is more than ten times higher (3300 kgCO_{2eq}/t). These numbers
441 have to be compared with the 522 kgCO_{2eq}/t and 1048 kgCO_{2eq}/t for the natural gas-based DRI
442 and the coal-based, respectively. Concentrated solar power could replace the energy required
443 to heat the ore and melt the DRI. The lower limit for the emissions is calculated by assuming
444 that the solar concentrator would have zero emissions on its entire life cycle. This would drop
445 the global emissions by 30%, reaching 210 kgCO_{2eq}/t and 2300 kgCO_{2eq}/t of steel for the French
446 and the Australian electricity mix, respectively. These basic calculations show that combining
447 concentrated solar power and green hydrogen production could drop the CO₂ emissions by at
448 most a factor 5 compared to coal-based DRI. It also illustrates that using hydrogen with an
449 electricity mix intensive in CO₂ is, on the contrary, of no interest.

450 IV. Conclusion

451 An alternative ironmaking process based on a concentrated light flux and hydrogen was studied
452 using industrial iron ore pellets. It was first demonstrated that the hydrogen pressure does not
453 have a strong impact on the dynamics of the process as long as the partial water vapor is kept
454 well below the one of hydrogen. It is also shown that using direct light as the heating source
455 induces a reduction mechanism different from the shrinking core model describing standard
456 processes: here, reduction starts from the illuminated surface towards the shadowed side, due
457 to the large temperature gradient inside the sample. This naturally conducted us to perform
458 experiments in which the pellets were rotated, consequently reducing exposure time. On single
459 pellets, a reduction yield of 96% was reached in 12 min by turning them three times during the
460 exposure. Other shapes of samples seem more suitable to a reduction under light flux than

461 spherical pellets so gravels and flat disks were tested. If the former did not lead to significant
462 improvement, results obtained on the latter were quite impressive: a 2 mm thick disk reached a
463 96% reduction yield after only 2 min of exposure.

464 Our results show that, for an efficient process, two parameters need particular attention : i) the
465 thickness of the sample (few millimetres depending on the power) and ii) the atmosphere
466 pressure ($H_2:Fe$ ratio needs to be at least 2.35:1) to avoid the re-oxydation. Additionally, it is
467 also shown that energy efficiency increases with both pressure and power. With these
468 considerations, for an optimized reactor, flat foils or chips of iron ore placed under the solar
469 flux might be a path to envisage. Optimizing such a process requires further simulations of the
470 gas diffusion as well as the temperature distribution into the sample. These points are currently
471 being studied by collaborators [42]. Once the reactor set and the process optimized, it will be
472 mandatory to perform life cycle assessments following several scenarios to study the potential
473 ecological advantage of this process.

474 The scale at which such a process could be advantageously envisaged is hard to determine. In
475 our view, such a solar process could only make sense in a society that seriously considers
476 sufficiency as a way to preserve human life as we know it as long as possible on our planet.
477 The “right” scale for this process should therefore be determined by considering the
478 geographical distribution of the production units and the global production level.

479 Acknowledgements

480 The authors thanks Marion Luu for her help in some experiments, Simon Cayez for XRD and
481 MAUD training, Touati Douar for mechanical and technical support, Catherine Crouzet for
482 electronics engineering and Stéphane Abanadès et Sylvain Rodat (PROMES lab, Odeillo,
483 France) for fruitful discussions. The authors also thanks ArcelorMittal for the raw material
484 supply. This study has been supported by the Agence Nationale de la Recherche (contract ANR-
485 20-CE05-0008-03, METASOL) and INSA Toulouse for the funding of B. Sanglard’s PhD.

References:

- 487 [1] World Steel association, ‘Steel’s contribution to a low carbon future and climate resilient
488 societies’, 2017, [Online]. Available: [https://www.steel.org.au/getattachment/48e75f3b-](https://www.steel.org.au/getattachment/48e75f3b-e33c-43e3-b3e8-b07b330293ae/Position_paper_climate_2017.pdf)
489 [e33c-43e3-b3e8-b07b330293ae/Position_paper_climate_2017.pdf](https://www.steel.org.au/getattachment/48e75f3b-e33c-43e3-b3e8-b07b330293ae/Position_paper_climate_2017.pdf)
- 490 [2] L. Holappa, ‘A General Vision for Reduction of Energy Consumption and CO₂ Emissions
491 from the Steel Industry’, *Metals*, vol. 10, no. 9, p. 1117, Aug. 2020, doi:
492 10.3390/met10091117.
- 493 [3] Z. Fan and S. J. Friedmann, ‘Low-carbon production of iron and steel: Technology
494 options, economic assessment, and policy’, *Joule*, vol. 5, no. 4, pp. 829–862, Apr. 2021,
495 doi: 10.1016/j.joule.2021.02.018.
- 496 [4] J. Astier, ‘Réduction directe’, *Techniques de l’ingénieur Métaux ferreux : élaboration du*
497 *métal primaire*, vol. base documentaire : TIB366DUO., no. ref. article : m7580. Editions
498 T.I., 2005. [Online]. Available: [https://www.techniques-ingenieur.fr/base-](https://www.techniques-ingenieur.fr/base-documentaire/materiaux-th11/metaux-ferreux-elaboration-du-metal-primaire-42366210/reduction-directe-m7580/)
499 [documentaire/materiaux-th11/metaux-ferreux-elaboration-du-metal-primaire-](https://www.techniques-ingenieur.fr/base-documentaire/materiaux-th11/metaux-ferreux-elaboration-du-metal-primaire-42366210/reduction-directe-m7580/)
500 [42366210/reduction-directe-m7580/](https://www.techniques-ingenieur.fr/base-documentaire/materiaux-th11/metaux-ferreux-elaboration-du-metal-primaire-42366210/reduction-directe-m7580/)
- 501 [5] T. Ariyama and M. Sato, ‘Optimization of Ironmaking Process for Reducing CO₂
502 Emissions in the Integrated Steel Works’, *ISIJ Int.*, vol. 46, no. 12, pp. 1736–1744, 2006,
503 doi: 10.2355/isijinternational.46.1736.
- 504 [6] H. Suopajarvi, E. Pongrácz, and T. Fabritius, ‘Bioreducer use in Finnish blast furnace
505 ironmaking – Analysis of CO₂ emission reduction potential and mitigation cost’, *Appl.*
506 *Energy*, vol. 124, pp. 82–93, Jul. 2014, doi: 10.1016/j.apenergy.2014.03.008.
- 507 [7] F. Patisson and O. Mirgaux, ‘Hydrogen Ironmaking: How It Works’, *Metals*, vol. 10, no.
508 7, p. 922, Jul. 2020, doi: 10.3390/met10070922.
- 509 [8] A. Heidari, N. Niknahad, M. Iljana, and T. Fabritius, ‘A Review on the Kinetics of Iron
510 Ore Reduction by Hydrogen’, p. 19, 2021.
- 511 [9] D. Wagner, O. Devisme, F. Patisson, and D. Ablitzer, ‘A laboratory study of the reduction
512 or iron oxides by hydrogen’, Aug. 2006.
- 513 [10] M. E. Choi and H. Y. Sohn, ‘Development of green suspension ironmaking technology
514 based on hydrogen reduction of iron oxide concentrate: rate measurements’, *Ironmak.*
515 *Steelmak.*, vol. 37, no. 2, pp. 81–88, Feb. 2010, doi:
516 10.1179/030192309X12506804200663.
- 517 [11] ‘MIDREX Process’, Midrex Technologies, Inc. Accessed: Apr. 07, 2023. [Online].
518 Available: <https://www.midrex.com/technology/midrex-process/>
- 519 [12] ‘Hybrit’, Hybrit. Accessed: Apr. 07, 2023. [Online]. Available:
520 <https://www.hybritdevelopment.se/en/>
- 521 [13] S. Hosokai, Y. Kasiwaya, K. Matsui, N. Okinaka, and T. Akiyama, ‘Ironmaking with
522 Ammonia at Low Temperature’, *Environ. Sci. Technol.*, vol. 45, no. 2, pp. 821–826, Jan.
523 2011, doi: 10.1021/es102910q.
- 524 [14] V. Vogl, M. Åhman, and L. J. Nilsson, ‘Assessment of hydrogen direct reduction for
525 fossil-free steelmaking’, *J. Clean. Prod.*, vol. 203, pp. 736–745, Dec. 2018, doi:
526 10.1016/j.jclepro.2018.08.279.
- 527 [15] World Steel association, ‘World steel in figures’, 2024.
- 528 [16] Ember, ‘Global electricity review 2024’, May 2024.
- 529 [17] M. Pathak, R. Slade, P. R. Shukla, J. Skea, R. Pichs-Madruga, and D. Ürge-Vorsatz,
530 ‘Technical Summary. In: Climate Change 2022: Mitigation of Climate Change.
531 Contribution of Working Group III to the Sixth Assessment Report of the
532 Intergovernmental Panel on Climate Change’. [Online]. Available: doi:
533 10.1017/9781009157926.002.

- 534 [18] A. Steinfeld and E. A. Fletcher, ‘Theoretical and experimental investigation of the
535 carbonthermix reduction of Fe₂O₃ using solar energy’, *Energy*, vol. 16, no. 7, pp. 1011–
536 1019, Aug. 1991, doi: [https://doi.org/10.1016/0360-5442\(91\)90061-P](https://doi.org/10.1016/0360-5442(91)90061-P).
- 537 [19] A. Steinfeld, P. Kuhn, and J. Karni, ‘High-temperature solar thermochemistry : Production
538 of iron and synthesis gas by Fe₃O₄-reduction with methane’, *Energy*, vol. 18, no. 3, pp.
539 239–249, 1993, doi: 10.1016/0360-5442(93)90108-P.
- 540 [20] D. Fernández-González, J. Prazuch, Í. Ruiz-Bustanza, C. González-Gasca, J. Piñuela-
541 Noval, and L. Verdeja González, ‘Iron Metallurgy via Concentrated Solar Energy’,
542 *Metals*, vol. 8, no. 11, p. 873, Oct. 2018, doi: 10.3390/met8110873.
- 543 [21] S. Li, H. Zhang, J. Nie, R. Dewil, J. Baeyens, and Y. Deng, ‘The Direct Reduction of Iron
544 Ore with Hydrogen’, *Sustainability*, vol. 13, no. 16, p. 8866, Aug. 2021, doi:
545 10.3390/su13168866.
- 546 [22] S. Abanades and S. Rodat, ‘Solar-aided direct reduction of iron ore with hydrogen
547 targeting carbon-free steel metallurgy’, *Renew. Energy*, vol. 235, no. 121297, 2024, doi:
548 <https://doi.org/10.1016/j.renene.2024.121297>.
- 549 [23] L. Brinkman, B. Bulfin, and A. Steinfeld, ‘Thermochemical Hydrogen Storage via the
550 Reversible Reduction and Oxidation of Metal Oxides’, *Energy Fuels*, vol. 35, no. 22, pp.
551 18756–18767, Nov. 2021, doi: 10.1021/acs.energyfuels.1c02615.
- 552 [24] L. Lu, J. Pan, and D. Zhu, ‘Quality requirements of iron ore for iron production’, in *Iron
553 Ore*, Elsevier, 2015, pp. 475–504. doi: 10.1016/B978-1-78242-156-6.00016-2.
- 554 [25] A. Ghosh and A. Chatterjee, *Ironmaking and steelmaking: theory and practice*, 3. print.
555 in Eastern economy edition. New Delhi: PHI Learning, 2010.
- 556 [26] J. Pang, P. Guo, and P. Zhao, ‘Reduction kinetics of fine iron ore powder in mixtures of
557 H₂-N₂ and H₂-H₂O-N₂ of fluidized bed’, *J. Iron Steel Res. Int.*, vol. 22, no. 5, pp. 391–
558 395, May 2015, doi: 10.1016/S1006-706X(15)30017-0.
- 559 [27] L. von Bogdandy and H.-J. Engell, *The Reduction of Iron Ores*. Berlin, Heidelberg:
560 Springer Berlin Heidelberg, 1971. doi: 10.1007/978-3-662-10400-2.
- 561 [28] O. Levenspiel, *Chemical reaction engineering. Hauptbd.*, 3. ed. New York Weinheim:
562 Wiley, 1999.
- 563 [29] A. Bonalde, A. Henriquez, and M. Manrique, ‘Kinetic Analysis of the Iron Oxide
564 Reduction Using Hydrogen-Carbon Monoxide Mixtures as Reducing Agent’, *ISIJ Int.*,
565 vol. 45, no. 9, pp. 1255–1260, 2005, doi: 10.2355/isijinternational.45.1255.
- 566 [30] D. Wagner, ‘Etude expérimentale et modélisation de la réduction du minerai de fer par
567 l’hydrogène’, Ph.D Thesis, Institut National Polytechnique de Lorraine, Nancy, 2008.
568 [Online]. Available: <https://hal.univ-lorraine.fr/tel-01753016/document>
- 569 [31] A. Ranzani Da Costa, ‘La réduction du minerai de fer par l’hydrogène : étude cinétique,
570 phénomène de collage et modélisation’, Ph.DThesis, Insitut National Polytechnique de
571 Laurraine, Nancy, 2011. [Online]. Available: [https://theses.hal.science/tel-](https://theses.hal.science/tel-01204934/file/These_Ranzani_2011.pdf)
572 01204934/file/These_Ranzani_2011.pdf
- 573 [32] D. Spreitzer and J. Schenk, ‘Reduction of Iron Oxides with Hydrogen—A Review’, *Steel
574 Res. Int.*, vol. 90, no. 10, p. 1900108, Oct. 2019, doi: 10.1002/srin.201900108.
- 575 [33] H. Lin, Y.-W. Chen, and C. Li, ‘The mechanism of reduction of iron oxide by hydrogen’,
576 *Thermochim. Acta*, vol. 400, no. 1–2, pp. 61–67, Apr. 2003, doi:
577 [https://doi.org/10.1016/S0040-6031\(02\)00478-1](https://doi.org/10.1016/S0040-6031(02)00478-1).
- 578 [34] C. Feilmayr, A. Thurnhofer, F. Winter, H. Mali, and J. Schenk, ‘Reduction Behavior of
579 Hematite to Magnetite under Fluidized Bed Conditions’, *ISIJ Int.*, vol. 44, no. 7, pp. 1125–
580 1133, 2004, doi: 10.2355/isijinternational.44.1125.
- 581 [35] E. T. Turkdogan and J. V. Vinters, ‘Gaseous reduction of iron oxides: Part I. Reduction of
582 hematite in hydrogen’, *Metall. Mater. Trans. B*, vol. 2, no. 11, pp. 3175–3188, Nov. 1971,
583 doi: 10.1007/BF02814970.

- 584 [36] G. Flamant, D. Gauthier, C. Boudhari, and Y. Flitris, ‘A 50 kW Fluidized Bed High
585 Temperature Solar Receiver: Heat Transfer Analysis’, *J. Sol. Energy Eng.*, vol. 110, no.
586 4, pp. 313–320, Nov. 1988, doi: 10.1115/1.3268273.
- 587 [37] S. Abanades, P. Charvin, and G. Flamant, ‘Design and simulation of a solar chemical
588 reactor for the thermal reduction of metal oxides: Case study of zinc oxide dissociation’,
589 *Chem. Eng. Sci.*, vol. 62, no. 22, pp. 6323–6333, Nov. 2007, doi:
590 10.1016/j.ces.2007.07.042.
- 591 [38] M. Neises, S. Tescari, L. de Oliveira, M. Roeb, C. Sattler, and B. Wong, ‘Solar-heated
592 rotary kiln for thermochemical energy storage’, *Sol. Energy*, vol. 86, no. 10, pp. 3040–
593 3048, Oct. 2012, doi: 10.1016/j.solener.2012.07.012.
- 594 [39] B. Sanglard, S. Lachaize, J. Carrey, and L. Tiruta-Barna, ‘Life cycle assessment of a
595 parabolic solar cooker and comparison with conventional cooking appliances’, *Sustain.*
596 *Prod. Consum.*, vol. 42, pp. 211–233, Nov. 2023, doi: 10.1016/j.spc.2023.09.018.
- 597 [40] IEA World Energy Statistics and Balances, ‘Ecoinvent 3.8 Dataset Documentation
598 “market for electricity, low voltage - FR - electricity, low voltage”’. OECD.
- 599 [41] IEA World Energy Statistics and Balances, ‘Ecoinvent 3.8 Dataset Documentation
600 “market for electricity, low voltage - AU - electricity, low voltage”’. OECD.
- 601 [42] A. Skaf, L. Tiruta-Barna, and A. Ahmadi, ‘Assessing the potential of low-temperature
602 ironmaking using pure hydrogen in shaft reactors’, *Submitted to Chemical engineering*
603 *and processing- Process intensification*, 2024.
- 604